MOON MINERALOGY MAPPER ANALYSIS OF VOLCANIC DEPOSITS IN SCHRODINGER BASIN.

M.J. McBride[1] B.H.N. Horgan[1] L.R. Gaddis[2] and K.A. Bennett[2]. [1]Purdue University, 610 Purdue Mall, West Lafayette, IN (mcbrid23@purdue.edu), [2]Astrogeology Science Center, U.S. Geological Survey, Flagstaff, AZ.

Introduction: Schrödinger is a 320 km diameter Imbrium-aged (~3.8 billion years old) impact crater located within South Pole-Aitken (SPA) basin on the lunar far side at 138ºE and 75º [1]. It is believed to be the second youngest basin on the lunar surface [2]. Pre-Nectarian-aged SPA basin is a 2400 km by 2050 km impact structure centered at −53°, 191°E on the far side [3]. Schrödinger is a target for future human or robotic exploration as its diverse lithologies would help address a variety of high priority lunar science goals. These include a conical edifice raised 415 m above the floor and an associated pyroclastic deposit with an area of 1250 km^2 located near the uplifted peak ring [4]. The proximity of these deposits would allow a robotic or human mission to answer questions about the history of both volcanic and impact processes in a single mission, which would address goals outlined in the Decadal Survey [5]. Since the relationship between the volcanic deposits in Schrödinger and the extent of the pyroclastic deposit with respect to the conical structure are not known in detail, we used spectroscopy and inferred mineralogy to assess the volcanic eruption style and history of the deposits.

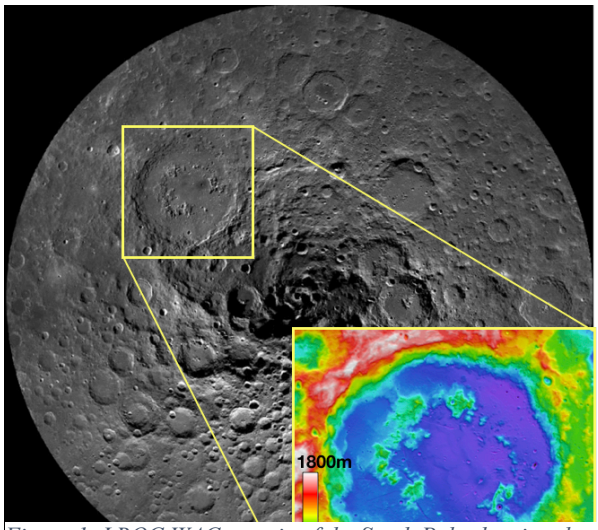

Figure 1: LROC WAC mosaic of the South Pole showing the location of Schrödinger basin. The inset displays the topography of the basin from LOLA data.

Background: Visible wavelength data (Figure 1) reveals that the pyroclastic deposits within Schrödinger crater may be relatively complex, with multiple pyroclastic deposits and an unusually high albedo compared to other lunar pyroclastic deposits [6]. Within SPA, the crust is thinner than typical lunar crust [7]. The Oppenheimer crater pyroclastic deposits, also located in SPA, exhibit diverse mineralogies consistent with a range of eruption styles beyond the Vulcanian eruption style previously hypothesized for these small deposits, including fire-fountaining and Strombolian [8]. Reduced crustal thickness in SPA may have created an environment that allowed magma to reach the surface more quickly, resulting in more volatile-rich eruptions [8]. Thus, it is possible that the pyroclastic deposits in Schrödinger also experienced a stronger pressure gradient during ascension, resulting in higher eruption rates than expected for other eruptions with the same volatile content.

Kramer *et al.* (2013) previously studies the Schrödinger basin with Level 1 M^3 hyperspectral data [9,10] by studying fresh material exposed by impact craters. The pyroclastic deposit was interpreted to be glass-rich, but the inner-Schrödinger mare could not be spectrally distinguished from the surrounding basin floor material [9]. Here we use Level 2 M^3 products, which include thermal and photometric corrections, incorporate spectra from outside of recent craters, and use more advanced mineral mapping techniques to expand on these earlier results and to determine the mineralogy and likely eruption style of Schrödinger pyroclastics.

Methods: M^3 was an imaging spectrometer on the Chandrayaan-1 lunar orbiter operating in the visible to near-infrared (0.42-3.0 μm). M^3 observations of the Schrödinger region have a resolution of 280 m/pixel in 86 spectral channels [10]. M^3 collected data during two operational periods distinguished by changes in instrument temperature and viewing orientation. Data for this project was obtained from optical period 2B. An M^3 map of the region was constructed with bounds 110-155ºE and 82-67ºN in an orthographic projection. The continuum of each spectrum was removed using a linear convex hull with two segments between 0.6-2.6 μm. Spectral noise was reduced using a median filter and a boxcar smoothing algorithm, both with widths of 5 channels [11,8].

Spectral diversity maps were created by applying spectral parameters to our M^3 mosaic. Our glass spectral parameter detects the wings of the glass iron absorption band, which is centered at much longer wavelengths than other Fe-bearing minerals, based on the average band depth below the continuum at 1.15, 1.18, and 1.20 μm [11]. Spectral parameters of the glass band depth, 1μm band center, and 2μm band center are mapped as red, blue, and green respectively in a composite image (Figure 2). Extracted spectra are visible in (Figure 3).

Results: Preliminary analysis of these M^3 data for Schrödinger basin (Figure 2) reveals that the volcanic terrains of the pyroclastic and the inner mare have a notably lower albedo than the surrounding terrain, and the color composite image highlights the mineralogical

diversity of the material in Schrödinger basin. Distinctive glass spectral signatures associated with the conical pyroclastic deposit that vary with distance from the vent and are especially strong to the southeast.

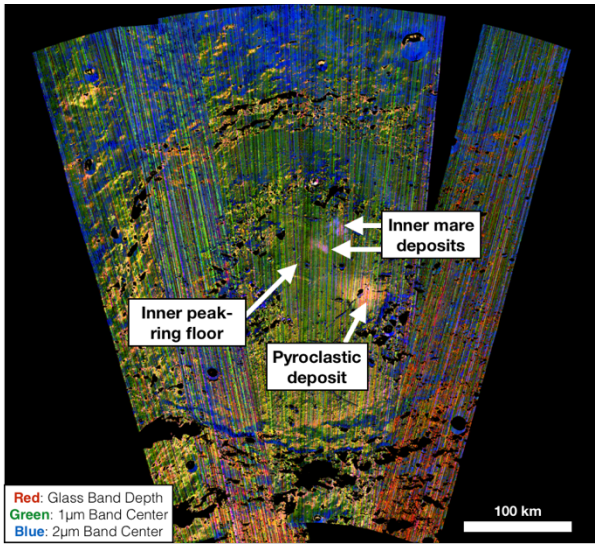

Figure 2: Composite RGB image of Schrodinger crater. Shades of yellow can be inferred as containing influence form glass while greens are dominated by orthopyroxene.

The M^3 extracted spectra (Figure 3) for Schrödinger units show distinctive iron-bearing absorption bands at 1000 and 2000 nm (1 and 2 µm). Spectra taken from the pyroclastic deposit indicate the presence of a mixture of glass and orthopyroxene that is consistent with an explosively emplaced volcanic deposit mixed with crater floor material, while the inner mare spectra are more consistent with clinopyroxene and minor glass, suggesting emplacement as a volcanic fissure eruption with possible associated effusion. Preliminary analyses also show spectral differences between the deposits created by impact and igneous processes and the inner-peak ring floor material. The inner mare is spectrally distinct from the inner peak-ring floor as well as the pyroclastic deposit. In future work, we will examine the band parameter maps and spectra for the pyroclastic deposit in more detail to assess their distribution relative to vents and local topography and to determine whether multiple eruptions may have occurred.

Discussion: The level 2 M^3 data and recently developed analysis techniques [11] have improved our ability to characterize mineralogies of geologic units within Schrödinger basin. These preliminary results of the spectral analysis of Schrödinger can be compared to analysis of the pyroclastic deposits in Oppenheimer crater [8]. Schrödinger has one large explosive deposit compared to the seven deposits in Oppenheimer associated with floor fractures. The largest deposit in Oppenheimer is comparable in size to the large deposit in Schrödinger, but is flat compared to the 415 m conical edifice. This is potentially due to material being erupted in one deposit compared to seven. The inner mare deposits of Schrödinger have a similar spectral signature of a clinopyroxene and glass mixture to some Oppenheimer floor deposits, both possibly be formed during a fire fountaining or Strombolian event where large blebs of molten magma accumulate near the vent and begin to form a lava flow and crystallize [8]. These results suggest that similarly complex volcanic eruption styles may have been typical among SPA pyroclastic deposits.

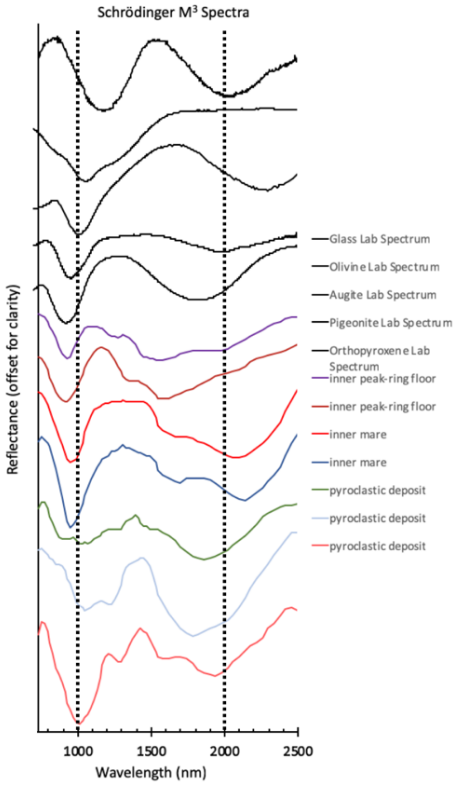

Figure 3: M^3 spectra extracted from the Schrödinger pyroclastic deposit, inner mare deposits, and inner peak-ring floor deposits compared to laboratory spectra.

References: [1] Wilhelms and McCauley (1971), [2] Shoemaker *et al.* (1994), *Science*, *266*(5192), 1851–1854. [3] Bethell and Zuber (2005), *GRL*, *32*(13), 2347, [4] Potts *et al.* (2014) *LPSC,* Abstract #1835. [5] National Research Council (2011) [6] Gaddis, L.R. et al. (2003) Icarus, 161:2, 262-280. [7] Wieczorek, M. A. *et al.* (2013), *Science*, 339(6120), 671–675 [8] Bennett et al. (2016) *Icarus*, 273, 296-314. [9] Kramer *et al.* (2013) *Icarus*, 223, 131-148. [10] Pieters *et al.* (2009), *Science,* 326, 568-572. [11] Horgan et al. (2014) Icarus, 234(C), 132–154.